Arbitrary waveform generation system using a quantum dash optical frequency comb source

Xie, Yuxuan; Khalil, Mostafa; Erfan, Touline; Liu, Jiaren; Lu, Zhenguo; Poole, Philip J.; Weber, John; Liu, Guocheng; Rahim, Mohamed; Chen, Lawrence R.

Publisher's version / Version de l'éditeur:
https://doi.org/10.1364/OPTCON.524839
Optics Continuum, 3, 8, pp. 1291-1301, 2024-07-25

Research Article Vol. 3, No. 8 / 15 Aug 2024 / Optics Continuum 1291
OPTICS CONTINUUM

Arbitrary waveform generation system using a quantum dash optical frequency comb source

YUXUAN XIE,[1,*] MOSTAFA KHALIL,[1] TOULINE ERFAN,[1] JIAREN LIU,[2] ZHENGUO LU,[2] PHILIP J. POOLE,[2] JOHN WEBER,[2] GUOCHENG LIU,[2] MOHAMED RAHIM,[2] AND LAWRENCE R. CHEN[1]

[1]*Department of Electrical and Computer Engineering, McGill University, 3480 University Street, H3A 0E9, Montreal, Canada*
[2]*Advanced Electronics and Photonics Research Center, National Research Council Canada, Ottawa, Canada*
[*]*yuxuan.xie@mail.mcgill.ca*

Abstract: We present an approach for microwave photonic (MWP) arbitrary waveform generation utilizing a quantum dash optical frequency comb source. Leveraging the availability of up to 41 comb lines and incorporating a real-time control feedback loop for precise comb shaping, we design a suite of MWP filters. Through the introduction of an ultra-short RF train, we obtain the impulse responses of the MWP filters, facilitating the construction of a versatile MWP arbitrary waveform generation system. In this study, we showcase the generation of rectangular, triangular, and sine burst waveforms. We can achieve an accuracy exceeding 90% in our generated waveform compared to the target waveform. Additionally, we demonstrate the tunability of the pulse width of rectangular and triangular waveforms, ranging from 0.62 ns to 4.56 ns, along with the adjustability of the triangular waveform slope. By manipulating the delay of the MWP filter, our system can also generate sine bursts, periodic sinusoids, and sinusoids with envelopes, with clock frequencies lower than that of the sinusoid itself.

1. Introduction

Arbitrary waveform generation (AWG) technology holds significant importance in various fields such as wireless communications, antenna and radar systems, and optical fiber communications. Microwave photonic (MWP) approaches have garnered interest due to their potential for ultra-large bandwidth (up to THz) and the feasibility of integration into compact chips [1]. Compared to the conventional electronic AWG systems, the main advantage of photonic approaches is its bandwidth. The maximum bandwidth of electronic AWG systems is usually limited by the speed of digital-to-analog converters (DACs), while the upper bandwidth of the photonic AWG system is dependent on the maximum bandwidth of the electro-optic modulators (EOMs) and photodiodes (PDs). State-of-the-art EOMs and PDs can achieve bandwidths of hundreds of GHz, even up to THz [2,3]. There are two typical approaches of MWP-AWG. The first method uses photonic up-conversion, where an electrical AWG generates the arbitrary waveform at a low bit rate, which is then up-converted to millimeter wave (mmWave) and THz ranges through techniques like heterodyne beating or higher-order harmonics [4–7]. Ensuring good phase characteristics during heterodyne beating necessitates optical sources with high phase performance, including low phase noise and frequency drift, with the possibility of phase-locking (when beating two wavelengths). The second approach involves spectrally shaping a broadband RF pulse, i.e., to tailor the impulse response of an MWP filter [1,8–13]. Typically, an MWP filter is realized as a digital finite impulse response (FIR) filter in the optical domain. One approach to implement a reconfigurable MWP filter requires an optical frequency comb (OFC) source to create taps with uniform comb spacing, a dispersion medium, and a programmable optical filter to control the power of each comb line. There are several approaches to generating OFC lines. The Kerr OFC

#524839 https://doi.org/10.1364/OPTCON.524839
Journal © 2024 Received 25 Mar 2024; revised 26 May 2024; accepted 27 Jun 2024; published 25 Jul 2024

OPTICS CONTINUUM

source utilizes a micro-ring resonator [14–16]. As a passive device, it necessitates an external pump laser. Although hybrid integration and photonic wire bonding technologies enable us to integrate the laser and the resonator on one chip, the non-flat optical spectrum is still the main limitation of Kerr OFC source. Another approach involves using cascaded EOMs, which offer a solution for tunable comb spacing [17–19]. While this cascaded EOM-based OFC source can achieve a flat comb spectrum and generate a large number of OFC lines [20–22], the main limitation is the need for multiple RF sources and/or careful synchronization amongst them. The last approach involves utilizing a mode-locked laser (MLL), such as quantum dash (QDash) and quantum dot (QDot) lasers [23,24]. In the context of MWP-AWG systems, the standout features of the MLL are its relatively flat comb spectrum and large numbers of comb lines. For instance, achieving perfect flat comb shaping with an MLL merely requires error compensation to reach the desired objective. Conversely, for non-flat OFC sources, all comb lines can be shaped down to the one with the lowest power. This suggests that MLLs offer greater flexibility and efficiency for comb shaping.

In this paper, we present experimental findings on MWP-AWG using a QDash MLL as the OFC source. Our system can generate individual or periodic rectangular and triangular waveforms. The parameters of the rectangular waveforms, including pulse width and period, are adjustable, while the edge slope and pulse width of the triangular waveform can also be modified. With minor adjustments to the system setup, we can extend its functionality to generate sine bursts and periodic sinusoids as well.

2. Quantum dash mode-locked laser

Figure 1(a) illustrates the cross-sectional view of the QDash laser utilize in this study. The core region of the QDash laser comprises a 350 nm InGaAsP layer hosting a five-layer InAs QDash structure with a periodicity of 108 Å, surrounded by a p-type InP cladding. Additional physical details regarding this laser can be found in [23,24]. The threshold current for the QDash laser is approximately 50 mA. With operational settings typically around 280-300 mA at 20°C, there is the production of 41 comb lines within the C-band with a comb spacing of 25 GHz (~0.2 nm), as illustrated in Fig. 1(b). The RF linewidth of this laser measures 9.98 ± 1.58 kHz; however, as our MWP-AWG system utilizes only optical intensity modulation, this linewidth does not influence our system performance. Instead, parameters such as relative intensity noise (RIN), comb power drift, and comb spacing are of significance. The average RIN for this laser is −130.5 dB/Hz, and the thermal comb power drift is approximately 0.15 dB. Lastly, the frequency drift of the comb spacing is within ±37.4 kHz, a value deemed negligible compared to the 25 GHz comb spacing.

OPTICS CONTINUUM

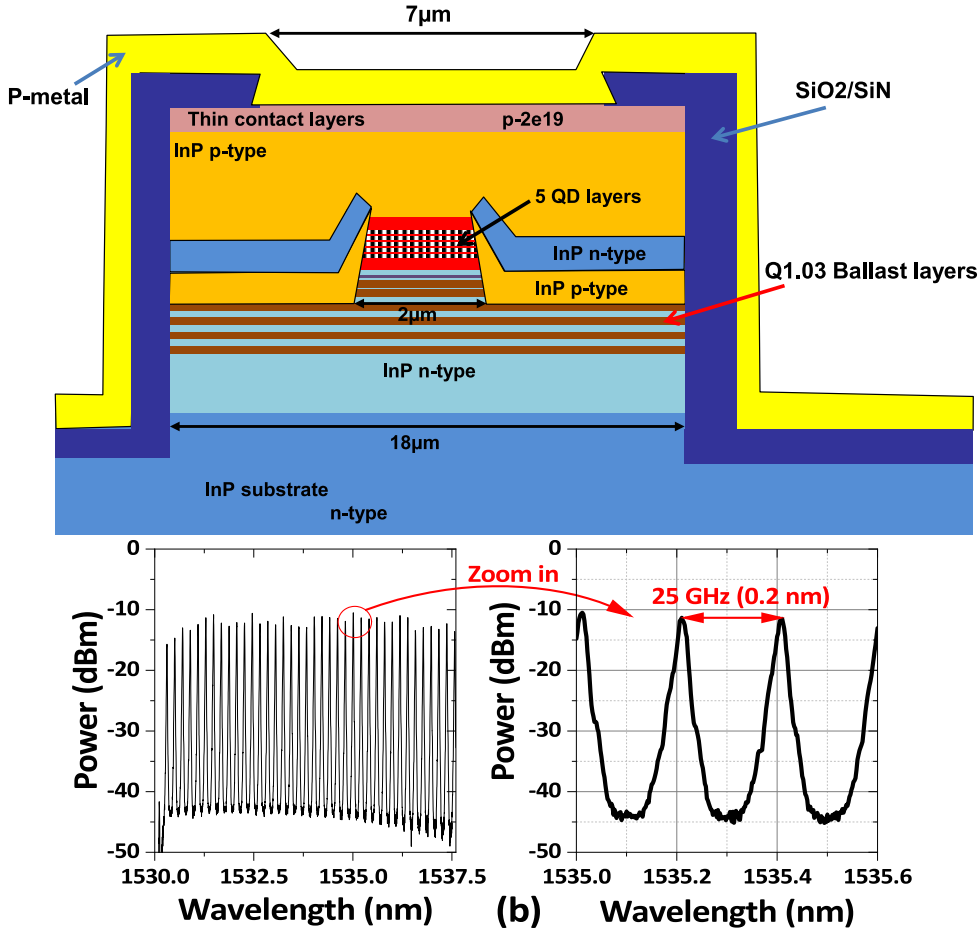

Fig. 1. (a) Schematic cross-sectional diagram of the QD laser [6]. (b) The optical spectrum of QDash laser with an injection current of 280 mA in 20 °C.

3. Principles, results, and discussions

The top part of Fig. 2 illustrates a general schematic diagram of the MWP filter. It is essentially an intensity-modulation direct detection (IMDD) system where the main difference is that it uses a multi-wavelength source instead of a single continuous-wave (CW) laser. The most important part of the MWP filter is comb shaping. Mathematically, the principle is the impulse response of an MWP filter. The frequency response of the OFC-based MWP filter is the discrete-time Fourier transform (DTFT) of the comb shaping matrix $p[n]$, which is also the main parameter that we can program. The matrix $p[n]$ represents the power of each comb line (note: $p[0]$ is the 1st comb line), which corresponds to the impulse response of the FIR filter. The total number of comb lines N is the order of the filter. T is the delay between two nearby taps, which is determined by the fiber dispersion D (in ps/nm) and comb spacing λ_{FSR}.

$$H(f) = \sum_{n=0}^{N-1} P(n) \exp[j2\pi nTf] = DTFT\{p[n]\}, \ where \ T = |D| \cdot \lambda_{FSR} \tag{1}$$

In our previous work [25,26], we presented some applications of MWP filters in the frequency domain. In this paper, the system is based on the impulse response of the MWP filters. As shown

OPTICS CONTINUUM

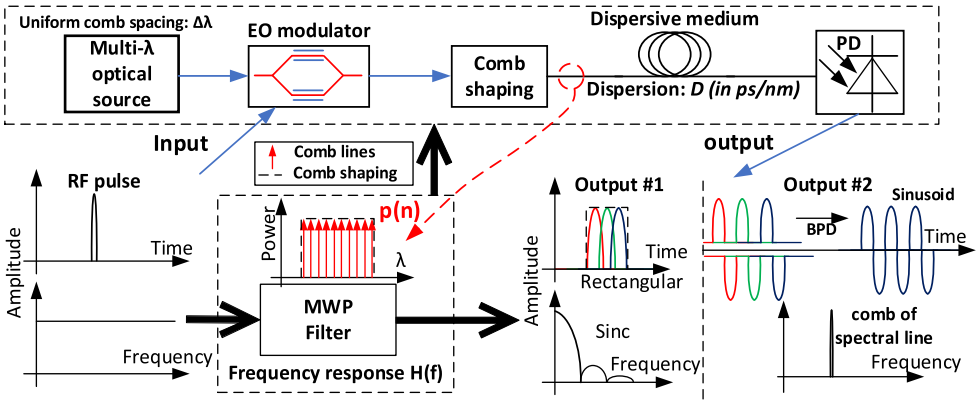

Fig. 2. Principle of MWP-AWG, where the first type output is based on a normal photodiode (PD) and a lowpass filter, and the second type output is based on a balanced PD (BPD).

in Fig. 2, the input is an ultra-short RF pulse in the time domain. By shaping the OFC lines with a rectangular window (i.e., flat shaping), the output of the MWP filter is a sinc function in the frequency domain, see Fig. 2 output #1. Therefore, by introducing an RF pulse as input, a rectangular impulse response is obtained. In practice, the system output can also be treated as the overlap of a set of delayed RF pulses, where the delay is from the fiber dispersion of the MWP filter. So, what we detect is the envelope of the delayed RF pulses. Moreover, the RF pulse is also periodic with a low repetition rate, which means that the spectrum is a comb of spectral lines with small period. Hence, the output spectrum of the MWP filter is a pulse train in the frequency domain, whose envelope is the *H(f)* in Eq. (1). Mathematically, the measured output of MWP filter with a RF pulse train input is the sampled *H(f)* in the frequency domain, where the sampling period numerically equals the frequency of the RF pulse train. Therefore, the measured spectrum is the discrete Fourier transform (DFT) of the comb shaping *p[n]*:

$$\begin{aligned} H_{measured}(f = kF_{pulse}) &= \sum_{n=0}^{N-1} p[n] \exp\left[\frac{j2\pi nk}{M}\right] \\ &= \sum_{n=0}^{N-1} p[n] \exp[j2\pi nTkF_{pulse}] = DFT\{p[n]\} \\ where\ M &= round\_down\left(\frac{1}{F_{pulse}|D|\lambda_{FSR}}\right),\ k\ is\ integer \end{aligned} \tag{2}$$

Equation (2) suggests that all measured spectra are discrete. Based on the sampling theory of DFT for a finite duration sequence, the length of DTF M must be greater or equal to the length of that sequence N, i.e., $1/F_{pulse}|D|\lambda_{FSR} \geq N$ (*total number of OFC lines*). It is important to note that an MWP filter is a pure analog system. Therefore, all terms relative to sampling are simply mathematical representations (there is no Nyquist rate in MWP-AWG systems).

All discussions above are based on the case when the delay ($|D|\cdot\lambda_{FSR}$) is less than the RF pulse duration. On the other hand, in scenarios where the delay is greater than the RF pulse duration, the RF pulses modulated on different taps experience separation (delay) due to fiber dispersion, resulting in noticeable gaps between them, as depicted in output #2 of Fig. 2. Nonetheless, by dividing the pulses into two branches, introducing a constant delay, and using a balanced photodiode (BPD) for detection, a sine burst waveform emerges. When introducing a pulse train input, this filter isolates a single frequency component, resulting in an output characterized by a comb of spectral lines in the frequency domain.

The experimental setup is depicted in Fig. 3. Overall, it is a combination of the upper part of Fig. 2 with some optical amplifiers and a control system. The electrical input of the optical

OPTICS CONTINUUM

modulator is a periodic train of short RF pulses, characterized by a full width at half maximum (FWHM) of 66.2 ps. The frequency of this pulse train is adjustable via a tunable clock. As previously mentioned, the output waveforms from the MWP-AWG system correspond to the two detectors shown in Fig. 3. When the delay of the taps is shorter than the pulse duration, a normal photodiode (as one branch of the balanced photodetector, Finisar BPDV21 × 0R) is required. Simultaneously, an electrical low-pass filter (LPF) with a cutoff frequency (f_{cut}) of 1.7 GHz is utilized to eliminate higher-order harmonics. It is important to emphasize that the MWP filter consistently governs the output waveforms due to the significantly higher frequency of f_{cut} compared to the waveform frequencies. The dispersion medium is a 40 km standard single-mode fiber (SSMF). For generating the sine burst waveform, the detector incorporates a BPD equipped with a 3-dB directional coupler and a pair of tunable delay lines (General Photonics VDL-001). Notably, the low-pass filter should be disconnected for the sine burst waveform. As previously discussed, the sine burst waveform necessitates longer taps delay, hence a dispersion compensating fiber (DCF) with |D|≈1371 ps/nm, equivalent to 80 km of SSMF, is connected this time. Finally, the form of the output waveform is ultimately determined by comb shaping. To facilitate this, a real-time feedback loop is established utilizing an optical spectrum analyzer (OSA) and a programmable optical filter (Waveshaper, Finisar 1000). Furthermore, during the creation of the sine burst waveform, the real-time oscilloscope (RTO, Tektronix DPO73304SX) can also be incorporated into the feedback loop to enhance accuracy.

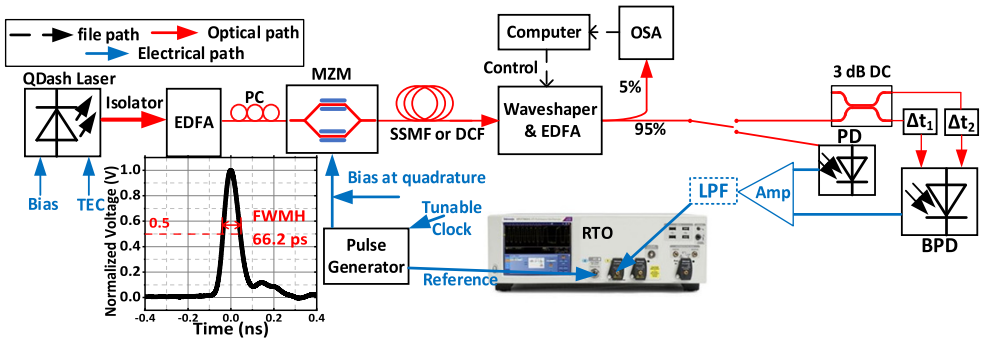

Fig. 3. Experiment setup of MWP-AWG system. TEC: thermoelectric controller, EDFA: Erbium-doped fiber amplifier, PC: polarization controller, SSMF: standard single mode fiber, OSA: optical spectrum analyzer, AMP: (electrical) power amplifier, LPF: (electrical) low pass filter, RTO: real-time oscilloscope.

We first focus on the generation of rectangular waveforms, with the desired shape determined by the comb shaping process. For a rectangular waveform, achieving a flat comb shaping is imperative. Despite having up to 41 quasi-flat comb lines available from the QDash laser, the power distribution among the comb lines varies, with the side comb lines exhibiting lower power compared to those in the central region. Considering the trade-off between total power and the number of comb lines, we opt to utilize a maximum of 35 comb lines for generating rectangular waveforms, as the total power is dictated by the comb line with the lowest power during flat shaping. Initially, we set the clock frequency to 10 MHz to isolate a single pulse, and the resulting waveforms are depicted in Fig. 4(a) and (b). By adjusting the number of comb lines, the width of the rectangular pulse ranges from 0.62 ns to 4.56 ns, with a step of 0.13 ns per comb line. Subsequently, we analyze the spectrum using the case of 20 comb lines as an example. As previously elucidated, the output spectrum of the MWP-AWG system is discrete. Thus, the spectrum shown in Fig. 4(b) comprises a comb of spectral lines, with a repetition rate equivalent to the clock frequency, and the envelope resembling a sinc function with a width of

OPTICS CONTINUUM

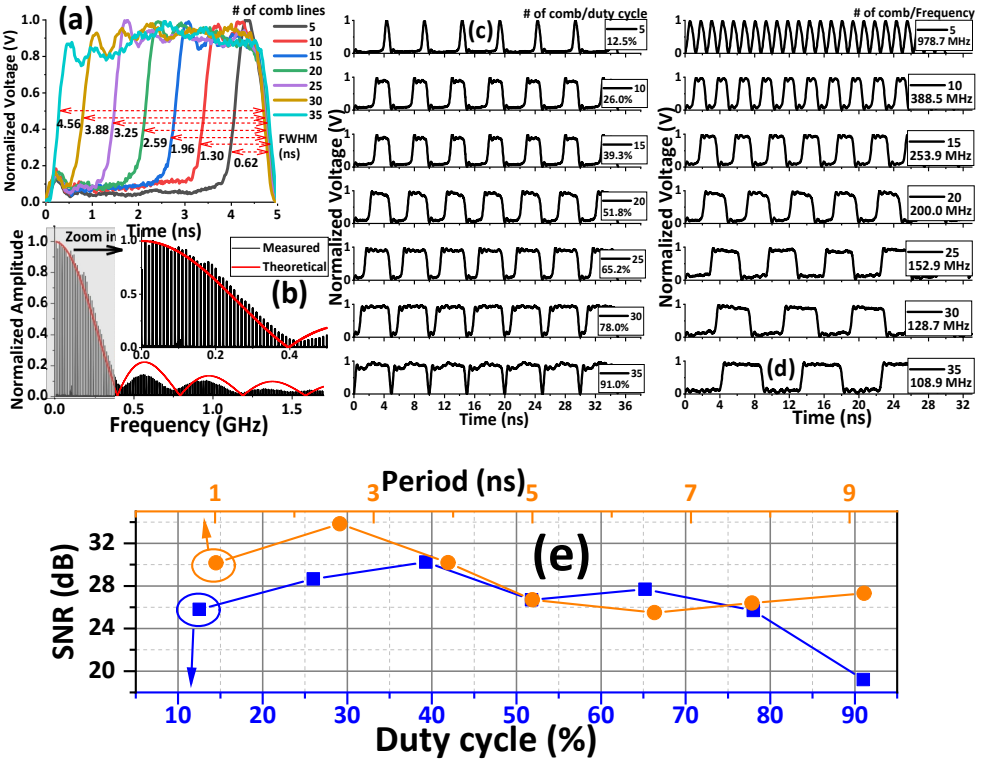

Fig. 4. Experiment results of (a) rectangular pulses with different pulse width, (b) the spectrum of the rectangular pulse with 20 comb limes, (c) 200 MHz periodic rectangular waveforms with different duty cycle, (d) periodic rectangular waveforms with different frequency, and (e) the signal to noise ratio (SNR) of waveform in (c) and (d).

386 MHz. The rectangular pulse illustrated in Fig. 4(a) serves as the fundamental unit of the periodic rectangular waveform. For instance, by fixing the clock frequency at 100 MHz, we obtain a series of 200 MHz rectangular waveforms with adjustable duty cycles, as demonstrated Fig. 4(c). Moreover, by ensuring that the clock period is always twice the width of the rectangular pulse, we achieve the generation of a periodic rectangular waveform, see Fig. 4(d).

Moreover, we conduct statistical analyses to evaluate the quality of the waveforms. These analyses are repeated numerous times, depending on the capture time of the RTO, with the case of 20 comb lines serving as an example here. Initially, we observe that the rising and falling times average at 417 ± 32.9 ps, primarily determined by the original edge time of the RF pulse (~44.5 ps) and the dispersion effects of the fiber (dominant). Additionally, the time jitter of the waveform is approximately 5.7 ps, where 2 ps jitter originates from the RF pulse generator based on datasheet specifications, while the remaining jitter is introduced by the MWP system. Finally, the signal to noise ratio (SNR) from the RF spectra of all demonstrated waveforms are shown in Fig. 4(e). When calculating the SNR, most of the comb of spectral lines are treated as signal, and the rest of the frequency components in the range of 0~33 GHz (the operating frequency range of our RTO) are considered as noise. Then, the signal and noise powers are calculated by integration based on their power spectral densities. Generally, the SNR is affected by two factors: the ASE noise of the EDFAs in the MWP system and the comb shaping. While more comb lines will allow us to generate more complex waveforms, it increase the difficulty of comb shaping. In this paper, the control loop of comb shaping is based on dB scale, and all waveform

OPTICS CONTINUUM

measurements are based on linear scale. Therefore, the error of comb shaping as well as power drift of the comb lines can affect the shape of the desired waveforms. The power drift of the comb lines is from the thermal instability of the QDash laser, which can only be controlled by the TEC.

In addition to rectangular waveforms, the MWP-AWG system can also generate triangle pulses and periodic triangle waveforms, utilizing principles analogous to those employed for rectangular waveforms. The main difference is in the comb shaping process, which this time adopts a triangular function under mW scale. Figure 5(a) illustrates a triangle pulse, serving as the fundamental unit of periodic waveforms. The slope and pulse width of the triangle pulse are controlled by the number of comb lines to the left and right of the peak, as indicated by the legends Fig. 5. Figure 5(b) displays the spectrum of the triangle pulse depicted in Fig. 5(a), showcasing a discrete spectrum with a sinc square envelope. By adjusting the total number of comb lines for the triangle waveform, the pulse width becomes tunable, consequently leading to a variable frequency ranging from 213.5 MHz to 1.21 GHz, as illustrated in Fig. 5(c). Furthermore, by maintaining the total number of comb lines at 41 and altering the location of the peak—e.g., 10/30 indicating the peak as the 11th comb line with 10 comb lines to the left and 30 to the right—a series of triangle waveforms with adjustable slopes are generated, as depicted in Fig. 5(d). Subsequently, we compare all results in Fig. 5(c) and (d) with a standard triangle waveform to assess performance, as summarized in Table 1, where the SNR is also included. The root-mean-square error (RMSE), expressed as a percentage since all waveforms are normalized, is utilized for evaluation. Initially, as the number of comb lines increases, the fidelity of the triangle waveform improves. However, beyond 26 comb lines, the feedback system encounters challenges in achieving the desired comb spectrum, resulting in degraded performance. Additionally, achieving sharp corners in the triangle waveform is challenging due to limitations imposed by harmonic terms; sharper corners correspond to poorer performance. This explains why the case of 20/20 in the tunable slope triangle exhibits the best performance.

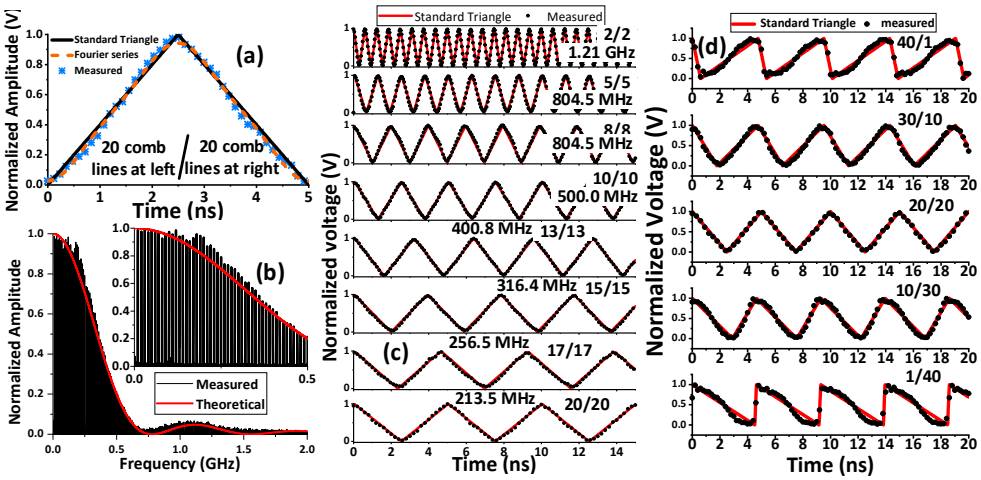

Fig. 5. Experiment results of (a) a standard triangle waveform, the measured triangle waveform, and its Fourier series fitting with 40 comb lines. (b) the spectrum of the triangle waveform with 40 comb limes, (c) periodic rectangular waveforms with different frequency, and (d) 213.5 MHz periodic rectangular waveforms with different slopes. Note: the legend means that the numbers of comb line on the left/right side of the peak.

The MWP-AWG system is also capable of generating sine burst waveforms, necessitating certain hardware modifications on the receiver side as depicted in Fig. 3. Initially, the light after the waveshaper is split using a 3-dB power splitter. Following the introduction of a delay on

OPTICS CONTINUUM

Table 1. The signal to noise ratio (SNR) of waveforms, and the root means square error (RMSE, normalized, %) compared to a standard triangle waveform.

Tunable frequency	2/2	5/5	8/8	10/10	13/13	15/15	17/17	20/20
RMSE (%)	7.15	6.16	5.14	2.61	2.17	2.69	2.75	3.01
SNR (dB)	33.02	29.58	25.93	30.73	30.36	30.03	29.15	28.05

Tunable slope	40/1	30/10	20/20	10/30	1/40
RMSE (%)	7.77	5.79	3.01	6.69	7.49
SNR (dB)	25.63	28.11	28.05	30.71	30.14

each branch, the light is detected by a BPD, without the use of a LPF after the power amplifier. This configuration represents output #2 in Fig. 2. Moreover, the delay between two adjacent taps must be equal to twice the pulse width. Therefore, with a 40 km SSMF, the waveshaper must be controlled to select one comb line from every three, resulting in a set of new OFC lines with a 75 GHz FSR and a total of 11 comb lines. The comb shaping for the sine burst waveform is flat. Figure 6(a) displays the measured sine burst waveform, represented by a first-order Fourier series to evaluate its performance. The repeat rate of the sine burst is 2.57 GHz, with a root mean square error (RMSE) of 8.72% compared to a standard sinusoid. Figure 6(b) illustrates the spectrum of the sine burst waveform. Since we split the taps before detection, the equivalent MWP filter resembles a 22nd order FIR filter with an impulse response alternating between +1 and −1. Consequently, the frequency response of the MWP filter exhibits a bandpass sinc filter with a center frequency equal to the repeat rate of the sine burst. Therefore, the spectrum in Fig. 6(b) consists of a comb of spectral lines with a sinc function envelope. By adjusting the clock frequency, the sine burst waveform can be rendered periodic, as depicted in Fig. 6(c). However, with a 40 km SSMF, the total number of taps is limited to 11. Increasing the fiber dispersion, such as by replacing it with a DCF ($|D|\approx 1371$ ps/nm), can reduce the FSR requirement to 50 GHz, which enable the use of up to 21 comb lines. Figure 6(d) discusses the required clock frequency, the SNR, and the RMSE with varying numbers of taps. More taps result in a lower clock frequency, dropping to 1/N of the sine wave frequency, where N is the total number of taps. This indicates the ability to generate a high-frequency signal with a low-frequency clock. However, more taps also present challenges for the control feedback loops, particularly for the comb lines on the side, leading to a deterioration in the RMSE and SNR of the sine waveform. Finally, the waveshaper allows for the programming of the sine waveform envelope. For instance, by shaping 11 taps into a triangle, a sinusoid with a triangular envelope is generated, as depicted in Fig. 6(e). With the DCF, 21 available taps offer more complex envelope options. For example, a sinusoid with a sinusoidal envelope is illustrated in Fig. 6(f), which is unattainable with only 11 taps.

The MWP-AWG system has the potential to generate more complex waveforms. However, it requires a multiport programmable optical filter (e.g., Finisar 4000 waveshaper) to create programmable positive and negative taps. Due to the unavailability of such hardware, we simulate the generation of more complex waveforms, and the results of which are shown in Fig. 7. By maintaining flat comb shaping and changing the arrangement of the positive and negative taps, a sine wave with a phase shift of π, e.g., as with phase-shift keying (PSK) is generated in Fig. 7(a). Moreover, the programable negative taps can also be used for envelope waveform generation. As illustrated in Fig. 7(b), by programing the comb spectrum, a chirped waveform can also be created.

The primary challenge and area for future improvement is comb shaping. Our experimental setup lacks polarization-maintaining components, leading to polarization fluctuations in the

OPTICS CONTINUUM

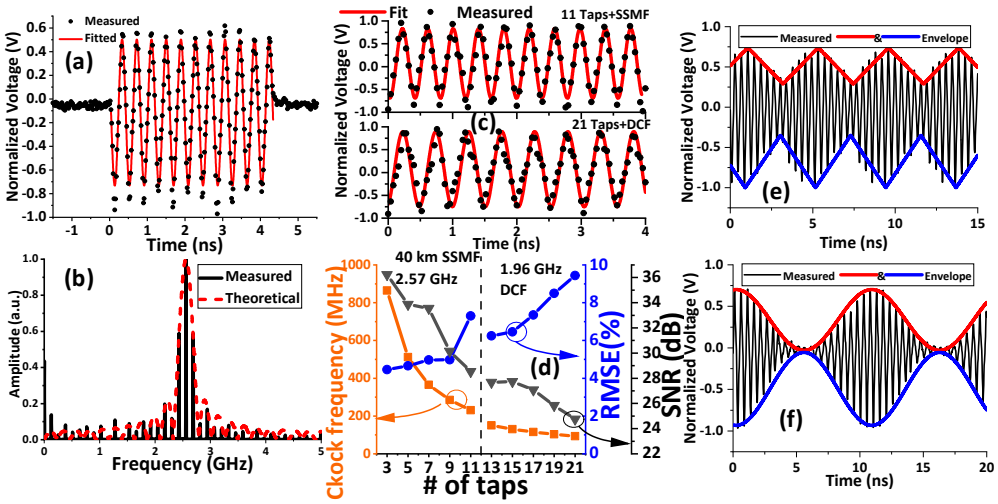

Fig. 6. Experiment results of (a) a sine burst waveform with 11 taps and 40 km SSMF, (b) the spectrum of sine burst, (c) periodic sine waveforms, (d) the requirement clock frequency the SNR, and RMSE with different taps, (e) a periodic sinusoid with a triangle envelope using 11 taps and 40 km SSMF, and (f) a periodic sinusoid with a sine envelope using 21 taps and DCF.

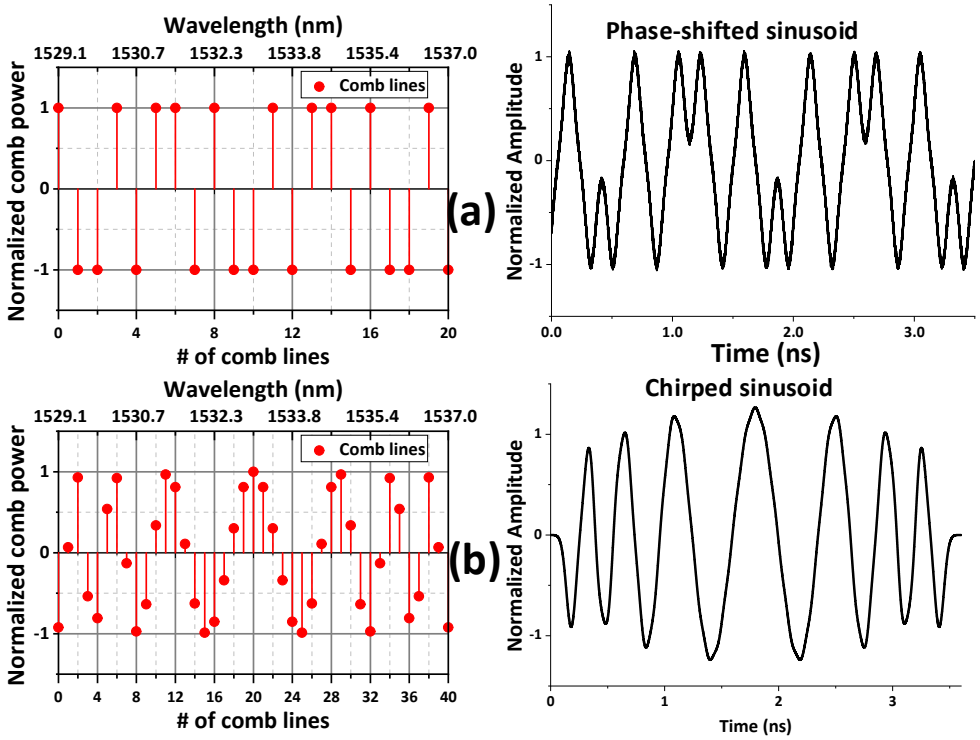

Fig. 7. Simulation results of (a) a phase-shifted sinusoid and its comb shaping, (b) a chirped sinusoid and its comb shaping.

OPTICS CONTINUUM

comb spectrum. These fluctuations increase the complexity of comb shaping, even when using a feedback loop, resulting in a greater error between the measured and desired comb shapes.

Additionally, the maximum operating frequency of our system is constrained by the width of the input RF pulse (the pulse shown in Fig. 3). The FWHM pulse width is 66.2 ps, corresponding to a maximum frequency of approximately 15 GHz (i.e., this is the available RF bandwidth to be filtered using the MWP filter for waveform generation). Increasing the bandwidth of the generated waveforms will require shorter input RF pulses. However, such shorter pulses will be more impacted by dispersion after E/O conversion (i.e., modulation onto the optical carriers). One possible solution is to use a pre-chirped RF pulse so that after E/O conversion, the broadening effect of fiber dispersion will be cancelled and the timed delay between taps (comb lines) can be maintained).

Finally, there is a trade-off between performance and programmability. Generating more complex waveforms requires a larger number of comb lines. However, increasing the number of comb lines also increases the error between the measured and expected comb shaping, leading to additional noise and distortion in the created waveforms.

4. Conclusion

This paper summarizes a programmable MWP-AWG system utilizing a QDash MLL as the OFC source. Leveraging the impulse response of an MWP filter, the system is capable of generating rectangular, triangular, and sine burst waveforms, with options for both pulse and periodic configurations. The abundance of comb lines provided by the QDash MLL, along with a programmable optical filter, enables tunability of the period and shape of the desired waveform. Notably, the pulse width of the rectangular and triangular waveforms is adjustable within the range of 0.62 ns to 4.56 ns, and the edge slope of the triangular waveform can also be modified. Through precise control of the delay between adjacent taps, the system can further generate sine burst and periodic sinusoids with programmable envelope characteristics.

Funding. National Research Council Canada.

Acknowledgments. We thank for the CMC Microsystems for providing the Rohde and Schwarz ZNB20 Vector Network Analyzer. This research was supported by the National Research Council Canada under project HTSN-206-1 and by the Natural Sciences and Engineering Research Council of Canada. The authors would also like to acknowledge Canadian Photonics Fabrication Center (CPFC) and Advanced Technology Fabrication (ATF) of the Advanced Electronics and Photonics (AEP) Research Centre at the National Research Council Canada for the material growth and device fabrication.

Disclosures. The authors declare that there are no conflicts of interest related to this paper.

Data availability. Data underlying the results presented in this paper are not publicly available at this time but may be obtained from the authors upon reasonable request.

References

1. C. L. Sung, C. Y. Lee, C. C. Chang, *et al.*, "Generation of terahertz optical beating from a simultaneously self-mode-locked Nd:YAG laser at 1064 and 1123 nm," Opt. Lett. **42**(2), 302 (2017).
2. E. Abacıoğlu, M. Grzeslo, T. Neerfeld, *et al.*, "500 GHz operational bandwidth MUTC-photodiodes with milliwatt terahertz output power levels," in *49th European Conference on Optical Communications (ECOC 2023)* (Institution of Engineering and Technology, 2023), pp. 1410–1413.
3. M. Burla, C. Hoessbacher, W. Heni, *et al.*, "500 GHz plasmonic Mach-Zehnder modulator enabling sub-THz microwave photonics," APL Photonics **4**(5), 056106 (2019).
4. X. Li, J. Xiao, Y. Xu, *et al.*, "QPSK vector signal generation based on photonic heterodyne beating and optical carrier suppression," IEEE Photonics J. **7**(5), 1–6 (2015).
5. Y. Li, Y.-W. Chen, W. Zhou, *et al.*, "D-Band mm-wave SSB vector signal generation based on cascaded intensity modulators," IEEE Photonics J. **12**(6), 1–8 (2020).
6. K. Zeb, Z. Lu, J. Liu, *et al.*, "InAs/InP quantum dash buried heterostructure mode-locked laser for high capacity fiber-wireless integrated 5 G new radio fronthaul systems," Opt. Express **29**(11), 16164 (2021).
7. D. Pérez-López, A. Gutierrez, D. Sánchez, *et al.*, "General-purpose programmable photonic processor for advanced radiofrequency applications," Nat. Commun. **15**(1), 1563 (2024).

OPTICS CONTINUUM

8. M. Tan, X. Xu, A. Boes, *et al.*, "Photonic RF arbitrary waveform generator based on a soliton crystal micro-comb source," J. Lightwave Technol. **38**(22), 6221–6226 (2020).
9. M. H. Khan, H. Shen, Y. Xuan, *et al.*, "Ultrabroad-bandwidth arbitrary radiofrequency waveform generation with a silicon photonic chip-based spectral shaper," Nat. Photonics **4**(2), 117–122 (2010).
10. H. Chi, C. Wang, and J. Yao, "Photonic generation of wideband chirped microwave waveforms," IEEE J. Microw. **1**(3), 787–803 (2021).
11. R. Adams, R. Ashrafi, J. Wang, *et al.*, "RF-arbitrary waveform generation based on microwave photonic filtering," IEEE Photonics J. **6**(5), 1–8 (2014).
12. R. Katti and S. Prince, "Microwave photonic system for ultrawideband waveform generation based on photonic microring resonator and electrical filter," in *2019 Workshop on Recent Advances in Photonics (WRAP)* (2019), pp. 1–3.
13. C. Song, S. Huang, X. Gao, *et al.*, "Photonics generation of baseband-free arbitrary-phase-coded microwave waveform pulse," IEEE Photonics Technol. Lett. **33**(9), 457–460 (2021).
14. X. Xue, Y. Xuan, C. Bao, *et al.*, "Microcomb-based true-time-delay network for microwave beamforming with arbitrary beam pattern control," J. Lightwave Technol. **36**(12), 2312–2321 (2018).
15. Y. K. Chembo, "Kerr optical frequency combs: theory, applications and perspectives," Nanophotonics **5**(2), 214–230 (2016).
16. T. J. Kippenberg, R. Holzwarth, and S. A. Diddams, "Microresonator-based optical frequency combs," **332**, (2011).
17. Z. Wang, M. Ma, H. Sun, *et al.*, "Optical frequency comb generation using cmos compatible cascaded Mach–Zehnder modulators," IEEE J. Quantum Electron. **55**(6), 1–6 (2019).
18. I. Morohashi, Y. Irimajiri, T. Sakamoto, *et al.*, "Generation of millimeter wave with high frequency accuracy using Mach-Zehnder-modulator-based flat comb generator," in *2012 IEEE International Topical Meeting on Microwave Photonics* (2012), pp. 35–38.
19. K. Zhang, W. Sun, Y. Chen, *et al.*, "A power-efficient integrated lithium niobate electro-optic comb generator," Commun. Phys. **6**(1), 17 (2023).
20. Y. Dou, H. Zhang, and M. Yao, "Generation of flat optical-frequency comb using cascaded intensity and phase modulators," IEEE Photonics Technol. Lett. **24**(9), 727–729 (2012).
21. S. Preussler, N. Wenzel, and T. Schneider, "Flexible Nyquist pulse sequence generation with variable bandwidth and repetition rate," IEEE Photonics J. **6**(4), 1–8 (2014).
22. R. Wu, V. R. Supradeepa, C. M. Long, *et al.*, "Generation of very flat optical frequency combs from continuous-wave lasers using cascaded intensity and phase modulators driven by tailored radio frequency waveforms," Opt. Lett. **35**(19), 3234 (2010).
23. Z. Lu, J. Liu, P. J. Poole, *et al.*, "InAs/InP quantum dash semiconductor coherent comb lasers and their applications in optical networks," J. Lightwave Technol. **39**(12), 3751–3760 (2021).
24. G. Liu, Z. Lu, J. Liu, *et al.*, "Monolithic InAs/InP quantum dash mode-locked lasers for millimeter-wave-over-fiber mobile fronthaul systems," IEEE J. Select. Topics Quantum Electron. **29**(6), 1–10 (2023).
25. H. Sun, M. Khalil, J. Liu, *et al.*, "Reconfigurable microwave photonic filter based on a quantum dash mode-locked laser," Opt. Lett. **47**(5), 1133 (2022).
26. Y. Xie, M. Khali, H. Sun, *et al.*, "Photonic beamforming using quantum-dash mode-locked frequency comb laser," in *2022 IEEE International Topical Meeting on Microwave Photonics (MWP)* (2022), pp. 1–4.